Design and Path Following Flight Test of a Flapping-Wing Air Vehicle

Sang-Gil Lee, Hyeon-Ho Yang, Hwankyun You, and Jae-Hung Han*
Korea Advanced Institute of Science and Technology, 291 Daehak-ro, Yuseong-gu, Daejeon, Republic of Korea

ABSTRACT

Flapping-wing air vehicles (FWAVs) have significant advantages in surveillance and reconnaissance missions due to their camouflage capabilities. In such missions, autonomous flight capabilities in outdoor environments are important. An FWAV capable of autonomous flight is designed in this research. The FWAV has elevons for generating pitching and rolling moments and can carry essential payloads such as the flight control computer (FCC) and GPS for outdoor autonomous flights. The flight test result demonstrates that the designed FWAV can autonomously follow a given circular path with implemented control method.

1 INTRODUCTION

Flying animals such as birds and insects have an excellent flight capability, allowing them to fly in forests and indoor environments. They have outstanding flight time and maneuverability compared to conventional aircrafts of similar size. These flying animals fly by flapping their wings, bio-inspired flapping-wing air vehicles (FWAVs) mimic this flight mechanism to pursue the flight capability of flying animals. Since FWAVs do not have a propeller rotating at high speed, they have many advantages, such as low noise and the ability to fly close to people. FWAVs also have the potential advantage that they can utilize various flight modes of flying animals, such as soaring, perching, and flap-gliding. In addition to these advantages, FWAVs are well-suited for surveillance and reconnaissance missions due to their excellent camouflage capabilities.

Insect-type FWAVs are advantageous for indoor environments with their hovering capabilities, and various studies have been conducted about their interesting aerodynamic [1, 2] and aeroelastic characteristics [3, 4]. On the other hand, bird-type FWAVs are more advantageous for outdoor missions in terms of payload capability and disturbance sensitivity than insect-type FWAVs. E-flap [5] is a bird-type FWAV developed with a focus on payload capability. The vehicle has achieved a payload capability of 520 g, which is close to its own mass. Meanwhile, SmartBird [6] focuses on mimicking the wing motion of real birds. It has multiple joints, so it can decrease downward force by reducing the wing area during the upstroke and can realize twist motion in the spanwise direction through an additional actuator.

The two above-mentioned FWAVs successfully achieved their goals, which are payload capacity and mimicking wing motion. However, the flight tests for those vehicles were conducted with manual control. Although autonomous flight has been performed in an indoor environment with small disturbance, the vehicle's positioning relied on an external device [7, 8]. Various control methods for FWAV have been proposed, but the number of studies that have successfully implemented control methods for outdoor flight is limited.

Dove [9] is capable of autonomous outdoor flight. Dove features a customized lightweight flight control system. The reason is that, considering Dove's specifications with a mass of 220 g and a wingspan of 50 cm, it is judged that the general electronic devices designed for unmanned aerial vehicles (UAVs) are not suitable in terms of their payload capability.

The vehicle developed in this research is focused on autonomous flight in the outdoor mission. It can carry a general flight control system for UAV (Pixhawk 4 mini and its GPS module), the control method for the path following is implemented, and a flight test is conducted to evaluate its performance in following a given path.

2 MATERIALS AND METHOD

2.1 *Hardware design*

The design mass is set based on the mass of electronics. The main electronics for outdoor autonomous flight are a flight control computer (FCC) and GPS. Pixhawk 4 mini, which is a general FCC for UAVs, and its GPS module are used. The masses of the FCC and GPS are 37 g and 33 g, respectively. In this study, the design mass is set at 700 g so that the electronics account for 10%, referring to the fact that electronics of Dove [9] and E-Flap [5] account for 16% and 11%, respectively. Wingspan can be calculated to be 1 m using $\mathrm{Wingspan} = 0.506 \cdot \mathrm{Weight}^{1/3}$ [10], and 1.2 m is selected to have a margin of 20%.

Before hardware design of the powertrain, it is necessary to determine the required power to select the proper motor for the powertrain. Firstly, wing kinematics is defined with the wing-fixed frame in Figure 1. The flapping angle ϕ refers to the x-axis rotation, and the twisting angle θ refers to the y-axis rotation. The flapping and twisting angles are assumed as follows:

*Email address(es): jaehunghan@kaist.ac.kr

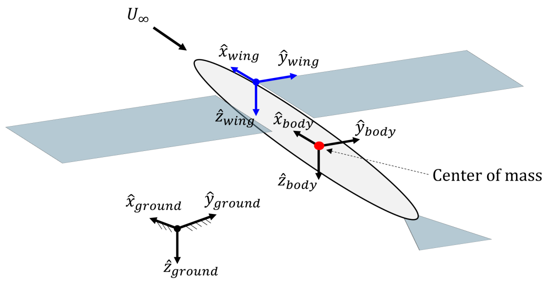

Figure 1: Reference frames of FWAV model

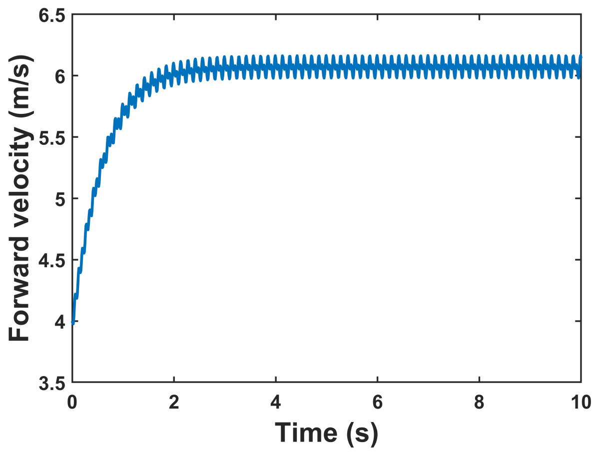

Figure 2: Converged forward velocity (Flapping frequency: 7 Hz, Twisting amplitude: 60°)

$$\phi_w(t) = \frac{\phi_{amp}}{2}\cos(2\pi f t) \tag{1}$$

$$\theta_w(t) = \frac{\theta_{amp}}{2}\sin(2\pi f t) \tag{2}$$

where ϕ_{amp}, θ_{amp}, f, and t represent flapping amplitude, twisting amplitude, flapping frequency, and time, respectively. Although the mechanism to be designed generates only flapping motion, the passive wing twisting induced by the structural deformation is assumed to have a 90-degree phase difference from the flapping motion.

The aerodynamic model used in this study is based on the quasi-steady aerodynamic model [11], and as a result, lift and drag coefficients are given as Equation 3 and 4. α represents the angle of attack in degrees. Each wing is discretized into multiple aerodynamic strips, and the aerodynamic loads on the strips are calculated with the lift and drag coefficients. Aerodynamic loads of each wing can be obtained by summing the lift and drag forces acting on the strips of the each wing.

$$C_L = 0.225 + 1.58\sin(2.13\alpha - 7.20) \tag{3}$$

$$C_D = 1.92 - 1.55\cos(2.04\alpha - 9.82) \tag{4}$$

To obtain the required power for the current FWAV with a 1.2 m wingspan, the flight dynamic simulations are conducted. The wing geometry used for analysis is simplified to a rectangular wing with an aspect ratio of 5, the simulation condition is that an pitch angle of body is 15°, and ϕ_{amp} is 45°. If only the x-axis of the ground-fixed frame has a degree of freedom, the forward speed converges to the trim state as represented in Figure 2. At this time, the cycle-averaged lift is calculated.

The results of flight dynamic simulation are shown in Figure 3. Assuming that the twisting amplitude is 40° or more, it can be confirmed that the flapping frequency need to be at least 7 Hz to generate lift greater than the design mass. The required power for flapping motion can be computed by multiplying the moment at the pivot point of the wing by the angular velocity, and the results are shown in the Figure 4. Because the maximum value of power consumption at 7 Hz is 109 W, the output power of motor should be greater than 109 W.

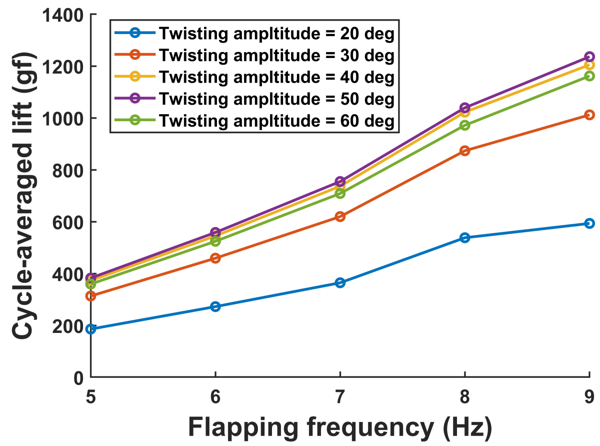

Figure 3: Cycle-averaged lift

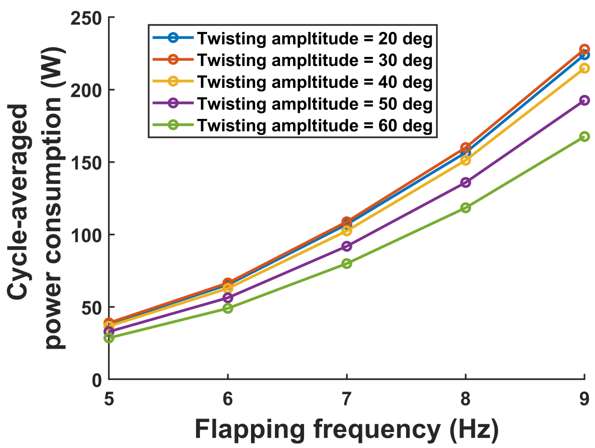

Figure 4: Cycle-averaged power consumption

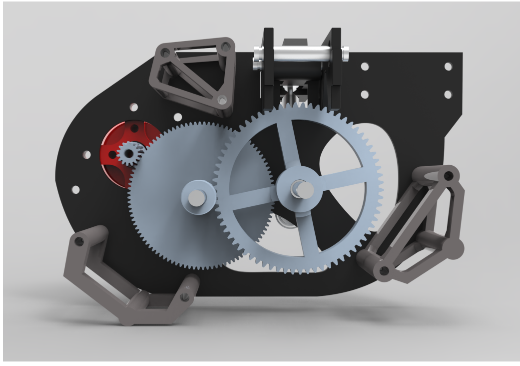

Figure 5: 2-stage gear train

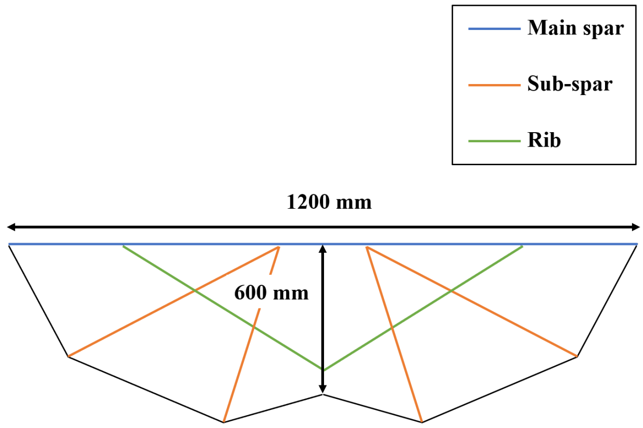

Figure 6: Geometry of main wing

A motor is selected with a margin considering factors such as transmission losses. The selected motor is a 1380 Kv brushless DC motor with a maximum output power of 178 W. The rotation speed of the motor is reduced with a 2-stage gear train. The first stage has a 6.67:1 reduction ratio, and the second stage has a 5.83:1 reduction ratio. The CAD model of the gear train is shown in Figure 5. The shaft of the gear train is supported by two side plates, which are 3D printed with Onyx from Markforged Inc. and represented in black color in Figure 5. Although carbon fiber-reinforced plastic (CFRP) plates can be used for the parts to reduce weight, this study opts for 3D printing for rapid prototyping. As the gear module increases, the size of the gear teeth also increases, enabling the gear to withstand higher contact forces. However, the gear radius also increases, resulting in an overall increase in the size of the mechanism. Because the first stage has a higher rotation speed and lower contact force between teeth than the second stage, the first stage has module 0.5 gears, and the second stage has module 0.8 gears. The output shaft of the gear train drives the revolute-spherical-spherical-revolute (RSSR) mechanism.

The main wing is connected to the RSSR mechanism and generates lift and thrust. The wingspan has been set to 1.2 as previously mentioned, and the geometry of the wing shape is shown in Figure 6. The coated fabric is used as a material for a wing sheet. The wing frame consists of main spars, sub-spars, and ribs, and it is fabricated using CFRP rods and pipes. The wing frame is attached to the wing sheet using adhesive tape.

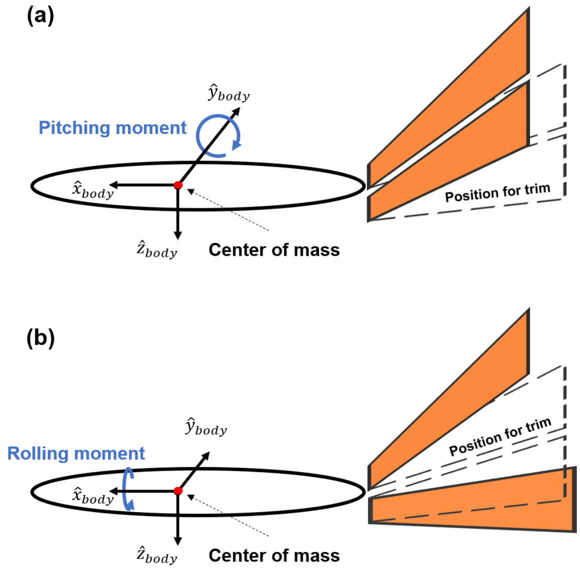

Figure 7: Configurations of elevons to generate control moment: (a) pitching moment; (b) rolling moment.

The tail wing is used for stabilization and control of FWAV. Configurations of control surfaces for FWAV are generally divided into two types: Elevons, and Rudder-elevator. Elevon is a compound word for elevator and aileron. The left and right horizontal control surfaces of the tail wing move independently. Therefore, they can generate pitching and rolling moments as shown in Figure 7. Rudder-elevator type is a common type for conventional aircraft. Pitching and yawing moments can be generated. Attaching control surfaces such as ailerons to the main wing of an FWAV is challenging because that the main wings have a flapping motion. As a result, roll stability relies on passive factors such as dihedral angles and the flapping counter-torque (FCT) [12]. In this study, the elevons are used as a control surface because active control of the roll direction rather than the yaw direction is considered to be more important.

The powertrain and the tail wing are connected using a CFRP pipe. The main wing is connected to the powertrain and the CFRP pipe. The CAD model of designed FWAV is shown in Figure 8. The fabricated FWAV in Figure 9 has a slightly higher mass than the design mass, and its specification is listed in Table 1.

Figure 8: CAD model of flapping-wing air vehicle

Figure 9: Fabricated flapping-wing air vehicle

Parameter	Value
Mass	740 g
Wingspan	1.2 m
Endurance	4 min
Aspect ratio	5.2

Table 1: Specification of flapping-wing air vehicle

2.2 *Controller*

Path following control is implemented based on the PX4 autopilot [13], open-source software. The overall structure of the control system is shown in Figure 10. The position controller in the total control system, is shown is Figure 11. Because the designed FWAV does not have a control surface for a yawing moment, the position controller only gives pitch and roll commands to the attitude controller, not the yaw command. It is assumed that yaw dynamics have enough stability from the flapping counter torque (FCT). The attitude controller has a cascaded loop structure. In an outer loop, angular rate setpoints are generated with attitude error. In an inner loop, the angular rate setpoints are tracked with proportional and integral (PI) feedback controllers and a proportional feedforward controller. For the details of guidance law and total energy control system, please refer to T. Stanstny and R. Siegwart [14] and A. A. Lambregts [15], respectively.

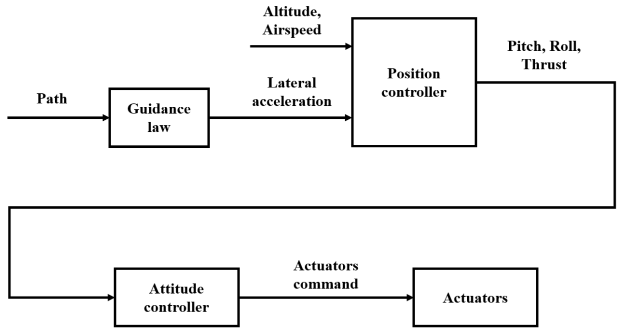

Figure 10: Overall structure of control system

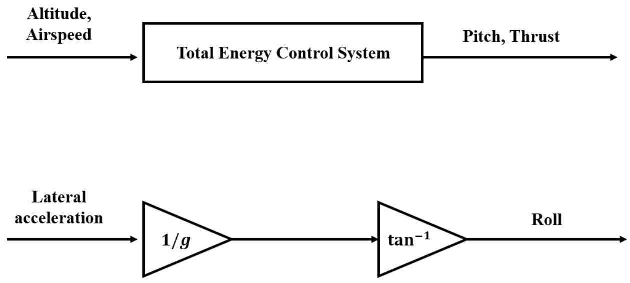

Figure 11: Position controller

3 FLIGHT TEST

The flight test was conducted to evaluate the performance of the designed FWAV and validate the implemented control method for autonomous flight. The flight test followed the sequence of takeoff, ascent, path following, descent, and landing. The FWAV was fully autonomously controlled during path following flight. Figure 12 shows a snapshot of conducted flight test, and the FWAV is highlighted with yellow circles.

The path following results are shown in Figure 13 and 14. The reference path was given as the circle with a 25 m radius and a constant altitude. The dashed line indicates the result of manual flight mode. In manual flight mode, only an attitude controller was active to track attitude commands given manually. After switching to the path following mode, the at-

Figure 12: Flight test snapshot

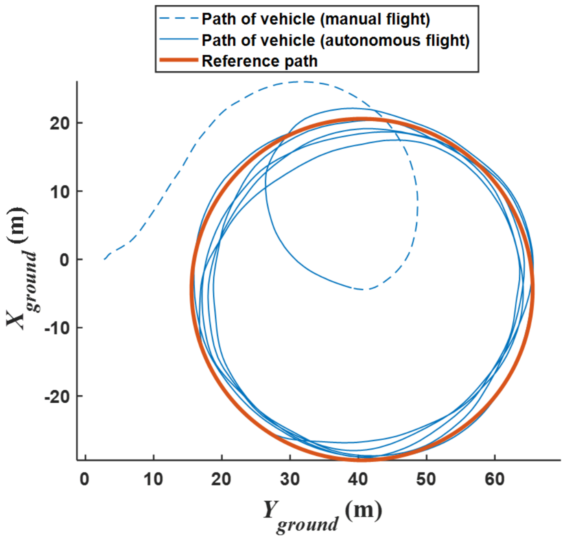

Figure 13: Path in horizontal plane

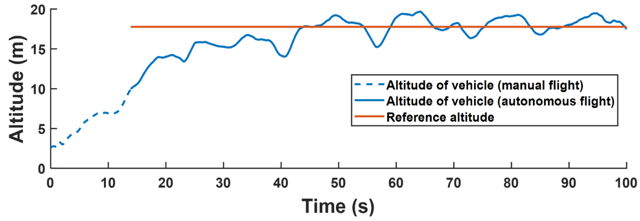

Figure 14: Altitude

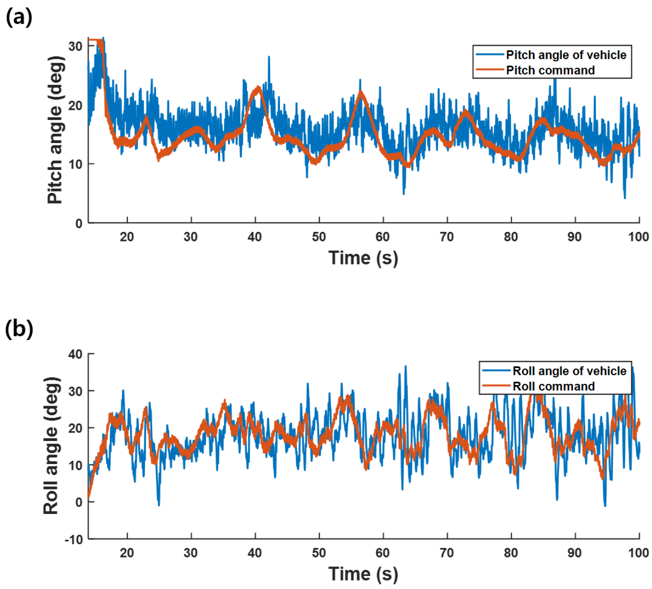

Figure 15: Attitude control result: (a) pitch angle; (b) roll angle.

titude commands were generated by position controller, and the attitude commands are shown in Figure 15. To follow the circular path in clock-wise direction, the roll command were given as a positive value. By tracking the attitude commands, the implemented controller successfully enabled the FWAV to follow the reference path.

4 Conclusion

In this study, the FWAV capable of autonomous flight was designed, and the flight test was performed to validate the implemented control method. The powertrain of the FWAV included a BLDC motor, a gear train, and an RSSR mechanism. The design of the powertrain was based on the established dynamics model. Elevons were chosen over the conventional rudder-elevator configuration due to their capability to generate rolling moments. To control the FWAV, which cannot generate a yawing moment, an appropriate control method was implemented based on the PX4 autopilot. The conducted flight tests demonstrated that the implemented control method can be successfully applied to the FWAV, enabling the FWAV to track the desired path.

The FWAV developed in this study has a relatively large size compared to the existing FWAVs designed for autonomous flight, allowing it to accommodate the avionics typically used in general UAVs. As a result, it is advantageous for outdoor missions. The designed FWAV is expected to be used as a test platform to validate the theoretically proposed control theories.

ACKNOWLEDGEMENTS

This research was supported by Unmanned Vehicles Core Technology Research and Development Program through the National Research Foundation of Korea (NRF) and Unmanned Vehicle Advanced Research Center (UVARC) funded by the Ministry of Science and ICT, the Republic of Korea (2020M3C1C1A01083415).

REFERENCES

[1] J.-S. Han, A. T. Nguyen, and J.-H. Han. Aerodynamic characteristics of flapping wings under steady lateral inflow. *Journal of Fluid Mechanics*, 870:735–759, 2019.

[2] A. T. Nguyen, J.-S. Han, and J.-H. Han. Effect of body aerodynamics on the dynamic flight stability of the hawkmoth manduca sexta. *Bioinspiration & biomimetics*, 12(1):016007, 2016.

[3] R. Addo-Akoto, J.-S. Han, and J.-H. Han. Aerodynamic characteristics of flexible flapping wings depending on aspect ratio and slack angle. *Physics of Fluids*, 34(5), 2022.

[4] A. T. Nguyen and J.-H. Han. Wing flexibility effects on the flight performance of an insect-like flapping-wing micro-air vehicle. *Aerospace Science and Technology*, 79:468–481, 2018.

[5] R. Zufferey, J. Tormo-Barbero, M. M. Guzmán, F. J. Maldonado, E. Sanchez-Laulhe, P. Grau, M. Pérez, J. Á. Acosta, and A. Ollero. Design of the high-payload flapping wing robot e-flap. *IEEE Robotics and Automation Letters*, 6(2):3097–3104, 2021.

[6] W. Send, M. Fischer, K. Jebens, R. Mugrauer, A. Nagarathinam, and F. Scharstein. Artificial hinged-wing bird with active torsion and partially linear kinematics. In *Proceeding of 28th Congress of the International Council of the Aeronautical Sciences*, volume 10. Brisbane, Australia, 2012.

[7] H.-Y. Kim, J.-S. Lee, H.-L. Choi, and J.-H. Han. Autonomous formation flight of multiple flapping-wing flying vehicles using motion capture system. *Aerospace Science and Technology*, 39:596–604, 2014.

[8] H.-Y. Kim, J.-S. Lee, and J.-H. Han. Indoor autonomous flight of ornithopter using motion capture system. *International Journal of Intelligent Unmanned Systems*, 1(3):204–214, 2013.

[9] W. Yang, L. Wang, and B. Song. Dove: A biomimetic flapping-wing micro air vehicle. *International Journal of Micro Air Vehicles*, 10(1):70–84, 2018.

[10] T. Liu. Comparative scaling of flapping-and fixed-wing flyers. *AIAA journal*, 44(1):24–33, 2006.

[11] M. H. Dickinson, F.-O. Lehmann, and S. P. Sane. Wing rotation and the aerodynamic basis of insect flight. *Science*, 284(5422):1954–1960, 1999.

[12] T. L. Hedrick, B. Cheng, and X. Deng. Wingbeat time and the scaling of passive rotational damping in flapping flight. *Science*, 324(5924):252–255, 2009.

[13] L. Meier, D. Honegger, and M. Pollefeys. Px4: A node-based multithreaded open source robotics framework for deeply embedded platforms. In *2015 IEEE International Conference on Robotics and Automation (ICRA)*, pages 6235–6240, 2015.

[14] T. Stastny and R. Siegwart. On flying backwards: Preventing run-away of small, low-speed, fixed-wing uavs in strong winds. In *2019 IEEE/RSJ International Conference on Intelligent Robots and Systems (IROS)*, pages 5198–5205, 2019.

[15] A. A. Lambregts. Vertical flight path and speed control autopilot design using total energy principles. In *Guidance and Control Conference*, page 2239, 1983.